www.cadanda.com
Computer-Aided Design AND APPLICATIONS™

Design and Development of Longitudinal and Torsional Ultrasonic Vibration-assisted Needle Insertion Device for Medical Applications

Yi Wang[1], Yi Cai[2] and Yuan-Shin Lee[3]

[1]North Carolina State University, ywang152@ncsu.edu
[2]North Carolina Agricultural and Technical State University, ycai@ncat.edu
[3]North Carolina State University, yslee@ncsu.edu

Corresponding author: Yuan-Shin Lee, yslee@ncsu.edu

Abstract. This paper presents a new design of longitudinal and torsional (L&T) ultrasonic vibration device for accurate needle insertion in medical applications. A waveguide-based Langevin type L&T ultrasonic transducer is proposed for the vibration-assisted insertion device. By cyclically altering the amplitude and direction of the resultant insertion speed, the proposed three-dimensional L&T ultrasonic vibration superimposed on the needle can reduce the friction force and needle bending during the insertion. Analytical modeling and analysis were conducted to study the vibration characteristics of the design. The new L&T ultrasonic transducer was fabricated using a metal 3D printing process. Laboratory experiments were carried out to validate the effectiveness of the new L&T vibration transducer design. The experiment results show the proposed new L&T vibratory needle insertion device is able to accurately deliver the insertion needle to the target depth and location. The presented new design and techniques can be used for medical treatments and implantation applications.

Keywords: Vibratory needle insertion, Biologically Inspired Design, Longitudinal-torsional vibration, Medical Applications, Finite Element Analysis
DOI: https://doi.org/10.14733/cadaps.2022.797-811

1 INTRODUCTION

Needle insertion as a medical procedure has been widely conducted for biopsy, brachytherapy, drug delivery, injection therapy, neurosurgery, medical treatments, etc. [1]. It is important for both patients and doctors to place the needle precisely on the treatment spots and to make it less painful as possible. The lower insertion force is capable of allowing for greater insertion precision and reducing patients' discomfort.

To improve needle insertion performance, vibration-assisted insertion as a dynamic insertion method has been researched and demonstrated useful. Currently, extensive research focuses on the

effect of the axial vibration on the needle insertion, showing a vibratory needle can effectively reduce the friction force and cutting force, thereby reducing the overall insertion force. Huang et al. [11] indicated high-frequency vibration reduces 28% of the friction and cutting force in needle insertion. Liao et al. [12] developed an ultrasonic device for needle insertion, which achieved 34% force reduction and 38% deflection reduction. They also reported that a larger amplitude vibration results in a lower insertion force. Barnett et al. [4], [17] reported that the insertion force can be reduced by as much as 35% using 25 μm peak-peak oscillation. Unfortunately, it is difficult to achieve high-frequency large-amplitude longitudinal ultrasonic vibration within a compact ultrasonic device due to its corresponding large mechanical impedance. While the insertion force is reduced by larger vibration amplitude and higher frequency, it has also been observed an unfavorable larger area of tissue damage and higher temperature generated during the insertion [17]. How to reduce the insertion tissue damages in surgery remains a major hurdle to be tackled.

To explore the potentials of vibratory needle insertion, the longitudinal vibration is extended to a three-dimensional vibration. Cleary et al. [9] developed a longitudinal-torsional ultrasonic device for bone biopsy to reduce forward force and increase precision than conventional longitudinal vibration. In their method, a modified a longitudinal-excited transducer structure was modified by cutting helical grooves around the circumference of the transducer while the inner cylindrical part remains solid. This type of transducers uses the partial reflection and superposition of the propagated waves to achieve hybrid vibration near the tip of the transducer [2]. One major drawback is that, with only modifyed external structure, it makes the axial vibration as the dominating factor to the combined vibrations hence its conversion effectiveness is limited. Although several other similar approaches have been used to guide the design of transducers, it remains an error-prone and tedious process to find the correct synchronous node planes for the combined tortional and longitudinal vibration modes. In our earlier works presented in [6], [7], a new design of longitudinal-flexing vibration surgical needle was developed by adding a series of micro slots on the needles. The experimental results demonstrated that three-dimensional vibration can further reduce puncture force and friction than using longitudinal vibratory needles. It still requires multiple iterations of design modifications and finite element simulations to arrive at an approprtiate needle vibration. Therefore, developing a three-dimensional vibration-assisted insertion device remains a necessary challenge to be overcome.

In this paper, we present a new longitudinal and torsional (L&T) ultrasonic vibration device to assist medical needle insertion. A waveguide-based Langevin type L&T ultrasonic transducer is designed, and 3D printed for the vibration-assisted insertion device. By using the superimposed L&T ultrasonic vibration and altering the insertion speed cyclically and instantaneously, it is our objective to further lower the friction force and needle bending. To compare and validate the effectiveness of the proposed L&T vibration, lab experiments were conducted and the results are discussed at the end of the paper. Details are presented in the following sections.

2 INFLUENCE OF ULTRASONIC VIBRATION ON NEEDLE INSERTION

During the needle penetration procedure, three primary force components act on the needle motion: cutting force, clamping force, and friction force, as shown in Figure 1. By analyzing the insertion force components, the friction force is the most influential factor during insertion, particularly as the needle penetrates deeper [15], [17]. During the insertion, the increased clamping force and the contact area between the needle surface and tissue rapidly increase the friction force, resulting in an increase in the total insertion force. Therefore, reducing the friction force is significant for lowering the total axial insertion force, thereby minimizing the tissue damage and deflection.

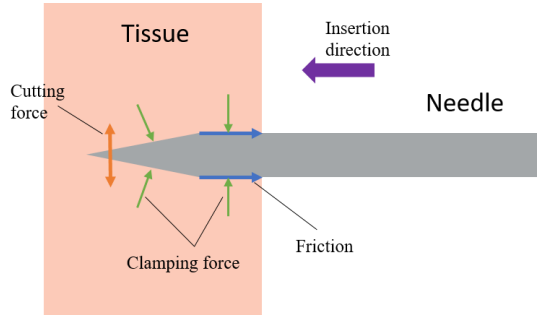

Figure 1: Forces during needle insertion.

According to the tribology research related to ultrasonic vibration, the macroscopic friction force reduction is influenced by the cyclic and instantaneous change of the resultant sliding velocity vector [10]. The friction force based on Coulomb's Law can be expressed as:

$$\overrightarrow{F_f} = -\mu_0 F_n \frac{\vec{v}}{|\vec{v}|} \tag{2.1}$$

where μ_0 is the coefficient of static friction, F_n is the pressure force acting on the needle, $\vec{v}$ is the resultant moving speed of the needle. To alter the resultant sliding velocity vector of the needle, an L&T ultrasonic vibration can be applied. When the L&T ultrasonic is superimposed on the inserting needle, the resultant velocity vector $\vec{v}$ of the needle can be derived from its displacement equation, as expressed in the following Equation (2.2). The resultant velocity vector $\vec{v}$ can be represented as two velocity components that are parallel ($\overrightarrow{e_x}$) and perpendicular ($\overrightarrow{e_y}$) to the needle insertion direction, shown as follows (also shown in Figure 2):

$$\vec{v} = \big(v_0 - A_L\omega cos(\omega t)\big)\overrightarrow{e_x} + A_T\omega cos(\omega t + \varphi)\overrightarrow{e_y} \tag{2.2}$$

where v_0 is the insertion velocity, A_L is the longitudinal vibration amplitude, A_T is the torsional vibration amplitude, ω is the vibration frequency, φ is the phase difference between the two vibration directions, $\overrightarrow{e_x}$ is the unit vector along insertion direction, and $\overrightarrow{e_y}$ is the unit vector perpendicular to the insertion direction. In Equation (2.2), the vibration velocities along the longitudinal and the torsional directions can be expressed as $A_L\omega$ and $A_T\omega$, respectively.

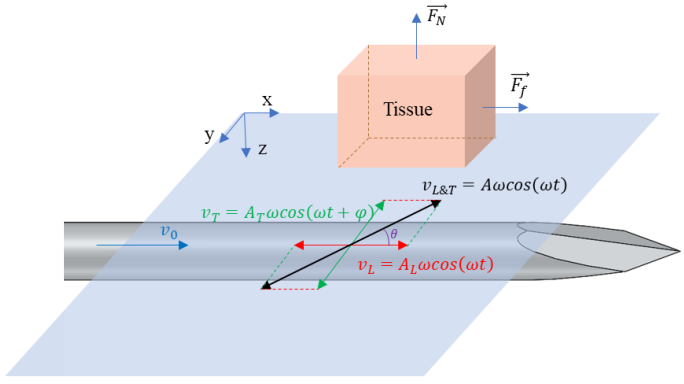

Figure 2: Illustration of velocity components of needle superimposed by L&T vibration.

Using Equations (2.2) and (2.1), the instantaneous friction force F_f along the insertion direction ($\overrightarrow{e_x}$) can be represented as:

$$F_f = -\mu_0 F_n \frac{v_0 - A_L \omega cos(\omega t)}{\sqrt{\left(v_0 - A_L \omega cos(\omega t)\right)^2 + \left(A_T \omega cos(\omega t + \varphi)\right)^2}} \tag{2.3}$$

The effective friction force to be measured is a time-averaged friction force $\overrightarrow{F_f}$[18], which can be calculated as follows:

$$\overrightarrow{F_f} = \frac{1}{T}\int_0^T f(t)dt \tag{2.4}$$

where T is the vibration period. By substituting Equation (2.3) to Equation (2.4), Littmann et al. [13] found that a friction force reduction can be formulated as a function related to a velocity ratio ξ defined as:

$$\xi = \frac{v_0}{A\omega} \tag{2.5}$$

where *A* is the actual amplitude of the L&T ultrasonic vibration. The instantaneous amplitudes along the longitudinal and the torsional directions can be represented as follows:

$$\begin{cases} A_L = Acos\theta \\ A_T = Asin\theta \end{cases} \tag{2.6}$$

where θ is the angle of vibration with insertion direction (see Figure 2). Using Equations (2.3) to (2.6), the friction force reduction ratio r can be calculated as:

$$r = \frac{1}{T}\int_0^T \frac{\xi - cos\theta cos(\omega t)}{\sqrt{\left(\xi - cos\theta sin(\omega t)\right)^2 + \left(sin\theta cos(\omega t)\right)^2}} dt \tag{2.7}$$

In the case of longitudinal only vibration ($\theta = 0°$), the friction reduction tends to not change ($r = 1$) when the velocity ratio ξ is larger than one ($\xi > 1$). According to Equation (2.7), even when the velocity ratio is greater than 1 ($\xi > 1$) and there is a non-zero angle θ between the vibration and the insertion direction ($\theta \neq 0°$, see Figure 2), the friction reduction can still be reduced. That means the direction change of the resultant velocity ($\theta \neq 0°$) causes further friction reduction ($r < 1.0$). To make such a change of the resultant velocity, in this paper, we propose to have an L&T ultrasonic vibration to be superimposed on the needle during the insertion, as shown earlier in Figure 2. In the next section, the design of such an L&T ultrasonic vibratory insertion is presented. To validate the effectiveness, the relation between the insertion force reduction rate (r) and resultant insertion speed (ξ) was studied in the experiments as presented in a later section.

3 DESIGN OF THE VIBRATION-ASSISTED NEEDLE INSERTION DEVICE

Figure 3 shows a design of a waveguide-based Langevin type L&T ultrasonic vibration device for needle insertion. The Langevin type transducer can achieve high electromechanical conversion efficiency and can only be excited by the axial polarized PZT ceramic stacks with a single ultrasonic driving power system. Some earlier L&T ultrasonic transducers were developed earlier by modifying the exterior of the transducer structures by machining with the inner cylindrical part remaining solid. It makes only the axial-direction vibration dominate the combined L&T vibration. Given such traditional structures, it is mathematically and realistically difficult to find the correct synchronous plane and the resonant frequency needed for both the longitudinal and the torsional vibration modes.

In our earlier work presented in [14], [20], the waveguide structure was developed and used in the ultrasonic transducer can directly guide the wave propagation direction with higher efficiency. As shown in Figure 3(a), an array of helical structures serving as waveguides is used in this paper to alter the longitudinal wave propagation thus achieve an L&T ultrasonic vibration. To achieve the desired wave propagation direction, the wave propagation path needs to be first defined.

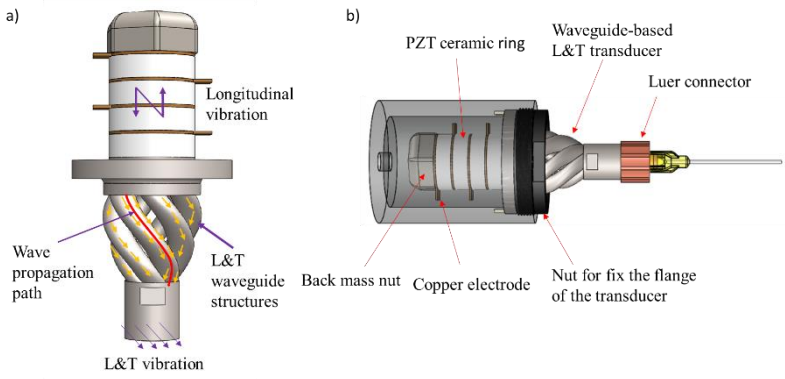

Figure 3: Design of the waveguide-based L&T ultrasonic vibration device: (a) illustration of the design of the L&T transducer, (b) assembly model.

As shown in Figure 3(a), a helical path was designed for the wave propagation path. A helical path $P(l)$ can be described as a circular helix in cylindrical coordinate, as follows:

$$\mathrm{P}(l) = \begin{cases} x(\alpha) = \dfrac{d}{2}cos\alpha \\ y(\alpha) = \dfrac{d}{2}sin\alpha, \qquad \alpha\epsilon[0,\pi] \\ z = \dfrac{L}{2\pi}\alpha \end{cases} \tag{3.1}$$

where d is the diameter of the circular helix, α is the rotational angle, and L is the height of the helix. And then, the waveguide structure can be defined as a wave propagation path $P(l)$ with an infinite number of cross-sections along and perpendicular to the path.

To achieve a high-efficiency L&T vibration at the output surface of the transducer, a circular array of such helix paths was designed. A hybrid L&T vibration is generated by the combination of a longitudinal force and a torsional moment. Using a waveguide to alter its direction, a longitudinal excitation can be partially transformed into a torsional moment, hence a combined longitudinal and torsional vibration. As presented in our earlier work in [20], [21], the exertion force F_{ext} and the exertion torsional moment M_{ext} at any point N along a waveguide path $P(l)$ can be calculated by applying Newton's second law to derive at the linear momentum and the angular momentum, as shown in Equations (3.2) and (3.3).

$$F_{ext} = \frac{\partial\left(\iiint \rho \frac{\partial \overrightarrow{u_N}}{\partial t} dV\right)}{\partial t} \approx -f^2\rho \iiint \overrightarrow{u_N}\, dV \tag{3.2}$$

$$M_{ext} = \frac{\partial\left(\iiint \rho \overrightarrow{GN} \times \frac{\partial \overrightarrow{u_N}}{\partial t} dV\right)}{\partial t} \approx -f^2\rho \iiint \overrightarrow{GN} \times \overrightarrow{u_N}\, dV \tag{3.3}$$

where ρ is the mass density of the waveguide material, V is the corresponding volume, vector $\overrightarrow{u_N}$ is the vibration displacement at any point N, $G \in P(l)$ the corresponding point along with the propagation path $P(l)$. In Equations (3.2) and (3.3), the derivative of time ($\partial/\partial t$) can be approximated as $1/\Delta t$, when the Δt is very small, and Equations (3.2) and (3.3) can be further simplified by using the ultrasonic frequency f that is proportional to $1/\Delta t$. What this means is the exertion force F_{ext} and the exertion torsion moment M_{ext} in Equations (3.2) and (3.3) can be further formulated as functions of the vibration frequency f. The resultant exertion forces $F_{ext_{end}}$ and the resultant exertion torsion moments $M_{ext_{end}}$ at the output surface of the transducer can be expressed as follows.

$$F_{ext_{end}} = \sum_{i=1}^{N} F_{ext_i} \tag{3.4}$$

$$M_{ext_{end}} = \sum_{i=1}^{N} M_{ext_i} \tag{3.5}$$

The appropriate output (exertion force $F_{ext_{end}}$ and exertion torsional momentum $M_{ext_{end}}$) of the proposed transducer for different applications can be controlled by using Equations (3.2)-(3.5). In this paper, a circular array of a total of six helical guides (N = 6 in Equations (3.4) and (3.5)) was used, to form a tapered shape L&T vibrator, as shown in Figure 3. The rotational angle α starts from 0 degrees and ends at 180 degrees. As shown in Figure 3, the tapered shape vibrator is able to boost the synchronous vibration to achieve a harmonic L&T vibration at the front output end.

Since the purpose of using our new design is to fit various types and sizes of needles, a commercial Luer connector was used, as shown in Figure 3(b). Base on the typical size of the commercial Luer connector, the diameter of the front end of the transducer was set as 10 mm. As shown in Figure 3, to reduce the overall size of the device and ensure the delivery of required vibration amplitude, we used four pieces of axial polarized Lead Zirconate Titanate (PZT-8) piezoelectric ceramic rings. The PZT-8 ceramic rings have an outer diameter of 15 mm and an inner diameter of 10 mm. Any two adjacent PZT-8 ceramics rings are oriented in the opposing direction. In the design, the copper electrode rings are alternatively sandwiched to connect the ultrasonic driving power. For safety concerns, the mass bolt and transducer are connected to the ground, and the adjacent pair of copper electrodes are connected to the ultrasonic driver. The piezo-ceramics stacks and copper rings are compressed by a 1045 steel heavy back mass nut to transfer wave forward efficiently. Since the compressing force will affect the vibration performance and efficiency, fine pitch threads are designed to control the applied compressing force. Based on the above critical sizes, the cross-section of each waveguide structure was set as 4.5 mm in diameter. An aluminum shell was designed to seal the piezoelectric ceramics. The flange of the transducer is compressed and fixed to the shell using a nut. The CAD model was built in the SolidWorks® 2020 [16] then imported to finite element analysis software ANSYS® 19.1 [3] for further optimization and vibration characteristics analysis, as discussed in the next section.

To be compared with the proposed L&T vibration, a traditional longitudinal vibration transducer, as shown in Figure 4, was also designed with the same critical dimensions. We adopted the same size flange and the same four pieces of PZT-8 ceramic rings. The total length of the transducer is also kept the same, only replacing the waveguide structures with a solid cylinder step. To ensure the two transducers have a similar resonant frequency, the diameter of the cylinder of the transducer was simulated multiple times and the correspondent parameters were adjusted till they have the identical vibration output signature. The resonant frequency and corresponding amplitude also were analyzed by using the finite element analysis software ANSYS® 19.1 [3]. Details are discussed in the next section.

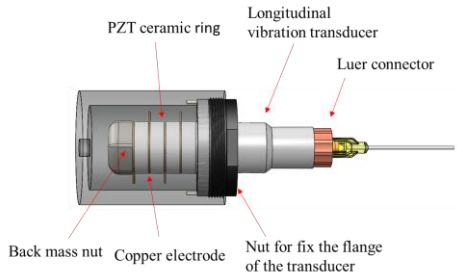

Figure 4: Illustration of the design of the traditional Longitudinal vibration transducer.

4 FINITE ELEMENT ANALYSIS OF THE L&T TRANSDUCER DESIGN

4.1 Finite Element Analysis Modeling

To optimize the proposed L&T vibrator design, harmonic response analysis was conducted to study the steady-state vibration behavior of the proposed vibration-assisted insertion devices. In this paper, the finite element analysis (FEA) software ANSYS® 19.1 [3] was used for the harmonic response analysis. The Piezo and MEMS module embedded in the ANSYS® Workbench [3] was adopted to simulate the exciting voltage applied to the piezoelectric ceramic rings, as shown earlier in Figure 3. The FE model was constructed for the CAD design of the waveguide-based L&T transducer with a 20 mm long blunt needle. Due to the complex geometric shape of the new transducer, the L&T transducer was fabricated with AlSi10Mg metal powders by using the Selective Laser Melting (SLM) 3D metal printing process. The SLM fabricated AlSi10Mg parts have a density of about 2670 kg/m^3 and its Young's modulus is 75 GPa. The traditional longitudinal transducer was machined with 6061 Aluminum with a density of 2700 kg/m^3 and Young's modulus of 76 GPa. The commercially available Lead Zirconate Titanate (PZT-8) piezoelectric ceramic rings were used in this paper, with a density of 7600 kg/m^3. Details of other parameters are shown in the following table, including the compliance matrix $[C^E]$, the piezoelectric coupling matrix $[d]$ and the relative permittivity matrix $[\frac{\varepsilon^T}{\varepsilon_0}]$ of the PZT-8 used in the FEA simulation.

Parameter	Value
Compliance matrix $[C^E]$	$\begin{bmatrix} 11 & -3.5 & -2.9 & 0 & 0 & 0 \\ -3.5 & 11 & -2.9 & 0 & 0 & 0 \\ -2.9 & -2.9 & 8.5 & 0 & 0 & 0 \\ 0 & 0 & 0 & 21 & 0 & 0 \\ 0 & 0 & 0 & 0 & 21 & 0 \\ 0 & 0 & 0 & 0 & 0 & 29 \end{bmatrix} * 10^{-12}\ m^2/N$
Piezoelectric coupling matrix $[d]$	$\begin{bmatrix} 0 & 0 & 0 & 0 & 450 & 0 \\ 0 & 0 & 0 & 450 & 0 & 0 \\ -100 & -100 & 225 & 0 & 0 & 0 \end{bmatrix} * 10^{-12}\ C/N$
Relative permittivity matrix $[\frac{\varepsilon^T}{\varepsilon_0}]$	$\begin{bmatrix} 1400 & 0 & 0 \\ 0 & 1400 & 0 \\ 0 & 0 & 1025 \end{bmatrix}$

Table 1: Material properties of PZT-8 for FEA model.

The heavy back mass nut is made of 1045 steel with a density of 7800 kg/m^3 and Young's modulus of 210 GPa. To simplify the FE modeling, four pieces of copper electrode rings were neglected in the FE electromechanical coupling model due to their thin thickness and lightweight. For the threaded connection in the model, we also replaced them with a bonded contact method in the ANSYS settings. A fixed constrain boundary condition was added to the flange region of the transducer.

4.2 Finite Element Analysis Results

Figure 5(a) shows the vibration amplitude response results versus the corresponding frequencies. It can be found that the peaks of both the longitudinal and the torsional vibrations have the same resonant frequency at 48.6 kHz. That means the longitudinal and torsional vibrations successfully resonate at the same time and frequency without any need for additional modification efforts, owing to using the proposed waveguide structure. At this resonant frequency, the combined L&T vibration can successfully be achieved. As shown in Figure 5(a), the amplitude of torsional vibration is slightly larger than that of the longitudinal vibration. Figure 5(b) shows the vibration displacements of the device generated by the FEA simulation software, at its corresponding resonant frequency. The needle was successfully driven to achieve a steady-state synchronized L&T vibration by the proposed

new design of the transducer. Importantly, the maximum L&T deformation appears at the tip of the needle, as shown in Figure 5(b).

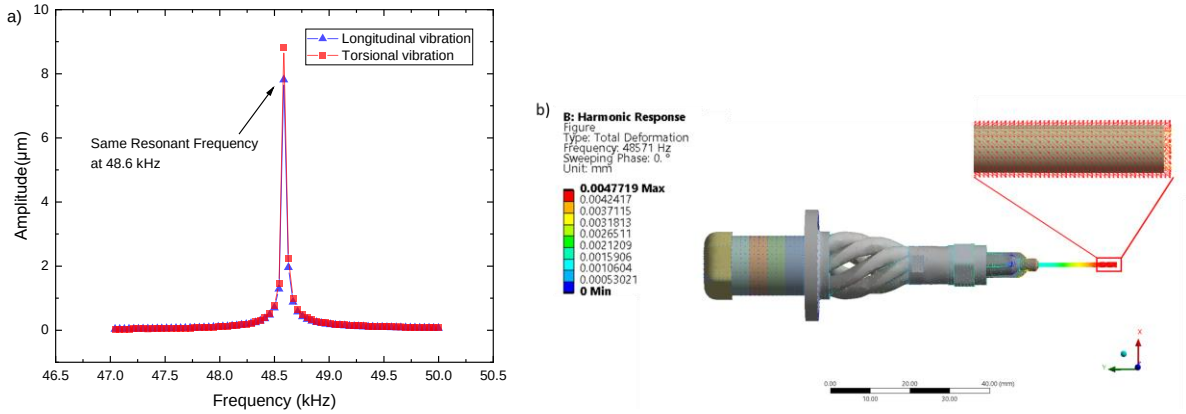

Figure 5: Harmonic response FEA simulation results of the proposed L&T vibration actuated needle: (a) vibration amplitudes versus sweeping frequencies, (b) vibration shape at the resonant frequency 48.6 kHz.

For comparison, Figure 6(a) shows the resonant vibration actuated by the traditional longitudinal vibration transducer. The structure has a similar resonant frequency at 50.6 kHz. Because of the long shaft topology of the needle, a longitudinal and lateral vibration was generated on the needle driven by a longitudinal-only vibrator. The reason for the needle having both longitudinal and lateral flexible vibrations results from one of the inherent modal shapes of the needle at a high frequency. To validate this point, the modal analysis of the needle used in the previous harmonic response analysis was also conducted to this traditional longitudinal vibration. As shown in Figure 6(b), the first-order modal shape of this needle is a longitudinal and lateral vibration that occurs at 54.1 kHz that is within the range of 45 kHz to 55 kHz (that is our working frequency band). Although the longitudinal and lateral vibration is also a three-dimension vibration, it is a kind of out-of-plane three-dimensional vibration compared to the in-plane L&T vibration. The impacts of the out-of-plane vibration still need to be further investigated. One of the concerns is that the lateral flexible vibration may enlarge the tissue opening during surgical insertion, causing unfavorable larger tissue damage. The flexing lateral vibration may also cause an insertion deflection due to the swing of the needle tip. These side effects will become severe when the needle is long and the vibration amplitude of the lateral vibration is large.

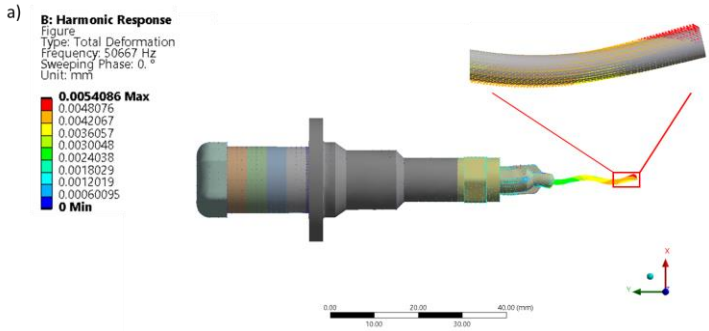

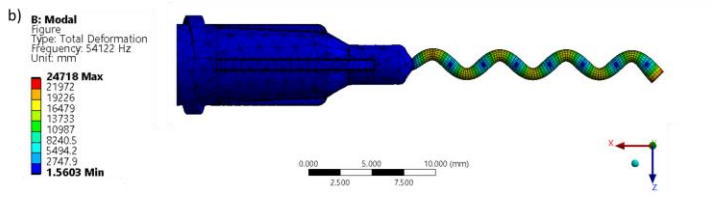

Figure 6: Finite element analysis results: (a) Harmonic response analysis simulation results of longitudinal vibration actuated needle, (b) Modal analysis of the needle itself.

5 FABRICATION OF THE PROTOTYPE

With the design geometric parameters being optimized with FEA analysis, the proposed L&T vibration-assist needle insertion device was fabricated for laboratory experiments. Due to the complex geometric design of the waveguide, the prototyped L&T transducer was fabricated with AlSi10Mg metal powders by using the selective laser melting (SLM) 3D metal printing process. Figure 7(a) shows the SLM 3D metal printed parts. The SLM fabricated parts have good mechanical properties and excellent fatigue performance, which can meet the dynamic characteristic required for ultrasonic vibration applications [5]. Because of the relatively rough surface finish of the as-built SLM components (±0.1 mm), the L&T ultrasonic transducer was first fabricated without the connecting holes and threads. Then a finishing operation was applied to only machining threads and flange region for assembly purposes. If needed, some additional potential finishing methods, such as electrochemical polishing or abrasive flow machining, could be possibly used in the future for a better finish. The Luer connector was assembled to the front end of the transducer by using threads. To compare with the proposed L&T ultrasonic vibration, a longitudinal vibration transducer made of Al 6061 was also machined by using conventional milling and turning operations. Figure 7(b) shows the longitudinal vibrator. The same four pieces of PZT-8 ceramic rings were used and clamped by a machined 1045 steel back mass nut, as shown in Figure 6(b).

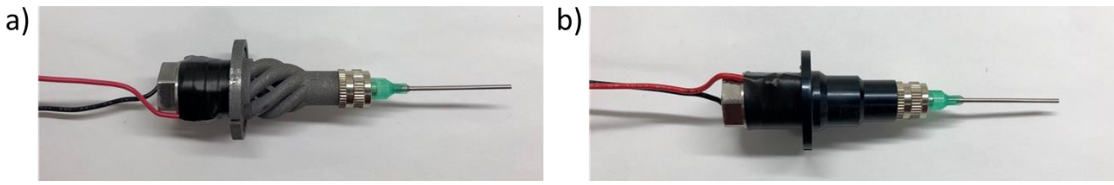

Figure 7: Prototypes of L&T ultrasonic transducer and longitudinal transducer.

6 LABORATORY EXPERIMENTS

6.1 Impedance Analysis

To validate the performance of the fabricated transducers, lab experiments were conducted. The impedance analysis of the transducers was carried out using the PiezoDrive® PDUS210 driver. As shown in Figure 8, the scanned frequency was specified from 20 kHz to 100 kHz. In the scanning period, the minimum impedance of both the proposed L&T transducers occurred at around 49 kHz, which are their corresponding resonant frequencies, as shown in Figure 8 (left diagram). This result also has a good agreement with the FEA results found to be at 48.6 kHz for the L&T transducer. For the traditional longitudinal transducer, the result is shown in the right diagram of Figure 8. The result of the traditional longitudinal transducer also agrees with the FEA result of 50.4 kHz. Since the two types of transducers have a similar resonant frequency, the superimposed vibration velocity can be changed by adjusting the driving voltage. Based on our earlier work presented in [14], [20], the

PZT-8 actuated Langevin type transducer has a good linear relation between the driving voltages and the vibration amplitudes.

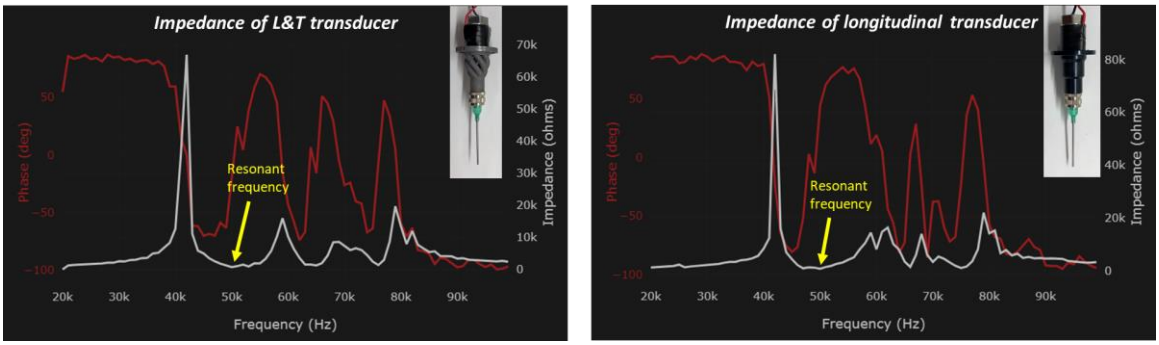

Figure 8: Impedance analysis of L&T ultrasonic transducer and longitudinal transducer.

6.2 Needle Insertion Experiments

Figure 9 shows the lab experimental setup for the vibratory needle insertion system. A six-axis force sensor (ATI® gamma series) was used to measure the insertion force at the rate of 60 Hz. A 3D printed plastic fixture was installed on the force sensor to secure a beaker with Gelly® wax phantom tissue. A linear motor (FUYU® FLS40) was programmable controlled using Raspberry Pi electronics. The assembled vibratory insertion device was eventually mounted on the linear guide with a 3D printed plastic fixture (see Figure 9). The PiezoDrive® PDUS210 driver was used to drive the ultrasonic device with adjustable variant voltages at the resonant frequency. During the insertion, the ultrasonic driver can continuously track the frequency shift to ensure that the ultrasonic device is operating at full performance.

It should be noted that when high power is applied to the transducer, the temperature at the Luer lock connector joint rapidly rises, due to the energy imposed on vibration. As shown in Figure 10(a), during the pexriments the vibration energy ventually melted the needle's plastic Luer lock connector. In the expiments, the max ultrasonic power is limited to 200 V. The temperature rose to 134 ^{o}C in 20 seconds as measured by FOTRIC 225 infrared camera, as shown in Figure 10(b). The reason is that the connection method of the Luer connector is by friction. Due to the large acoustic resistance of the interface between metal and plastic Luer connector, the high-frequency and large-amplitude vibration generate a lot of heat in the joint region. Also, the plastic connector used in the experiments has a lower thermal conductivity, causing a rapid temperature rise. To avoid this, in the future, the assembly design between the commercial needle and ultrasonic transducer can be optimized and the metal Luer connector could be used for similar ultrasonic applications. The experiment observation reflects the fact, during medical surgery, that vibration needles or tools could result in tissue damages due to both vibration force and thermal damages.

Figure 11 shows the insertion force measurement results with an 18G blunt needle at an insertion speed of 0.5 mm/s under the following conditions: (i) no vibration, (ii) longitudinal (L) vibration, (iii) combined L&T vibration. Three identical insertion phases (pre-puncture, puncture, and post puncture) were used for the observation. The measurement results are shown in Figure 11. Both the traditional longitudinal vibration and the proposed L&T vibration are able to lower the puncture force by about 36% and 38%, respectively. A smaller surface dimpling also can be observed under the influence of longitudinal vibration and L&T vibration before the needle puncturing the tissue. A larger surface dimpling area indicates larger tissue deformation and larger stored deformation energy, which results in a large puncture force and tissue damage after the puncture [8]. In the post-puncture phase (see Figure 11), the insertion force increases linearly. As shown in Figure 11, in this phase, the proposed combined L&T vibration reduces the maximum insertion force by 15%, compared with longitudinal vibration by 7%.

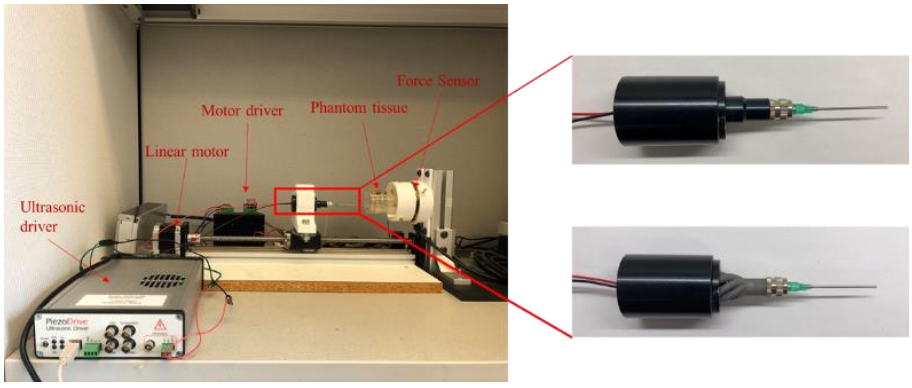

Figure 9: Experiment setup for vibration-assisted needle insertion.

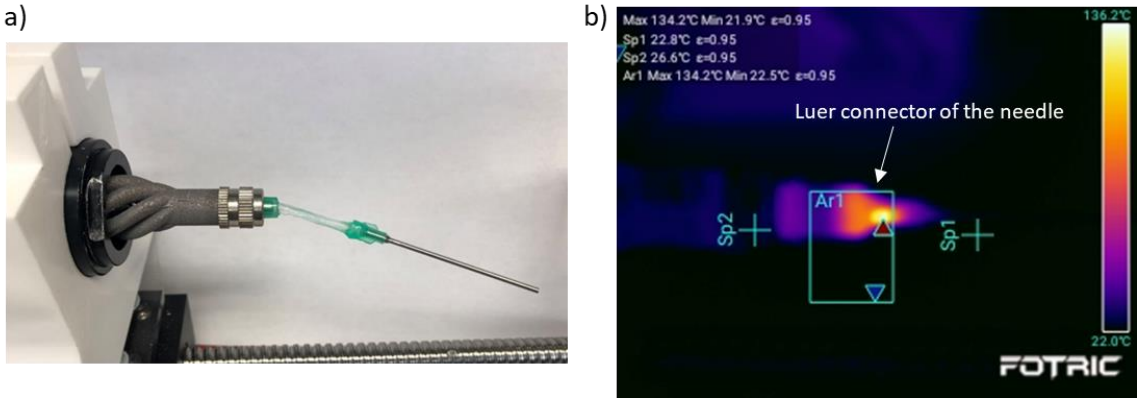

Figure 10: High power ultrasonic vibration causes the failure of the Luer connector of the needle.

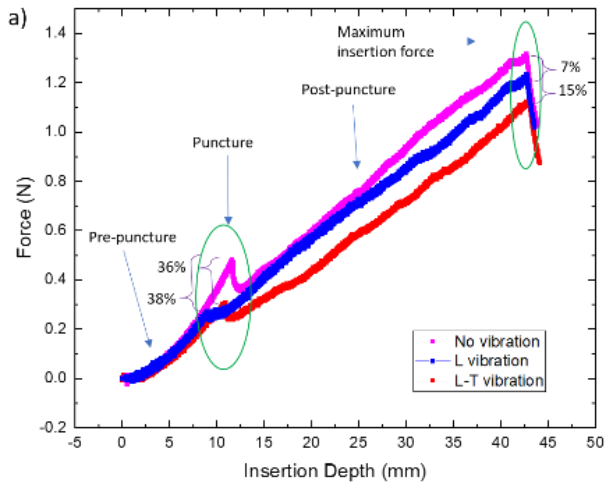

Figure 11: Insertion force measurement at 0.5 mm/s insertion speed.

To investigate the influence of ultrasonic vibration on the insertion force, the relationship between the insertion force reduction and the resultant insertion speed was studied through experiments. As

shown in Figure 12, a constant insertion speed at 1mm/s was used and only the driver's voltage was adjusted for variant L&T ultrasonic vibration velocity ($A\omega$). As shown in Figure 12, it can be found that the insertion force decreases rapidly with an increasing driving power voltage V.

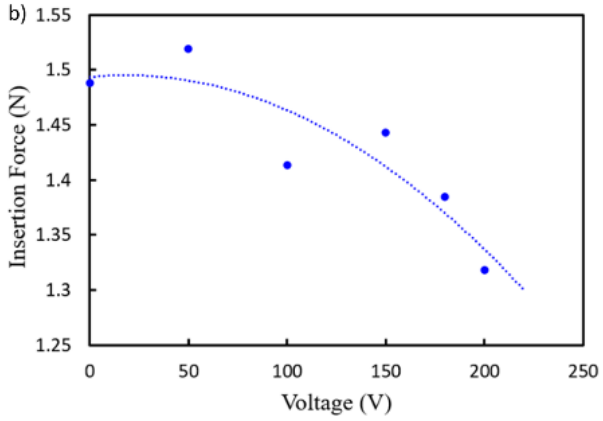

Figure 12: Insertion force at 0.5 mm/s versus driving voltage.

Given the friction force is affected by the velocity ratio ξ mentioned earlier in Equation (2.7), different insertion speeds were selected for experiments under three insertion scenarios (with traditional longitudinal vibration, with combined L&T vibration, and without vibration). The vibration power voltage was set at 200 V. For each condition, the experiments were repeated three times each for data sampling. Figure 13(a) shows the insertion experiment results performed with a gage 18G blunt needle. In Figure 13 (a), it is noticed that the insertion force reduction decreases as the insertion speed increases. Importantly, L&T ultrasonic vibration results in a lower maximum insertion force compared to the traditional longitudinal-only vibration, particularly when the insertion velocity is high. This observation also confirms our formulation in Equation (2.7). For comparison, we also used a commercial 18G sharp needle to verify the effects of different vibrations. The comparison results are shown in Figure 13(b). The proposed L&T vibration is able to reduce more insertion force than the traditional longitudinal-only vibration. During the insertion, the sharp needle causes a lower insertion force compared to the blunt needle. As the insertion speed increases, the ultrasonic vibration-induced force reduction weakens, similar to the use of blunt needles. That means when a velocity ratio ξ becomes large, the friction force reduction effect is reduced.

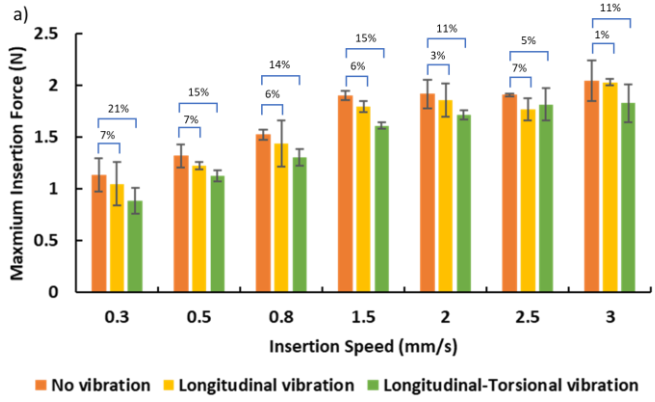

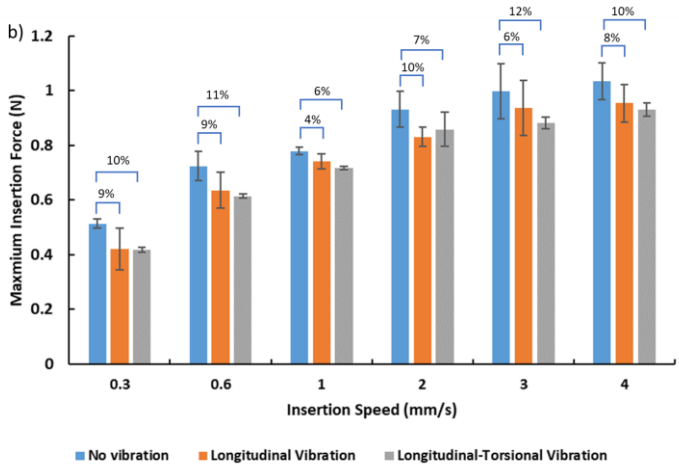

Figure 13: The maximum insertion force at different insertion velocities: (a) 18G Blunt needle (b) commercial 18G sharp needle.

To study the effect of insertion force on the bending of insertion trajectory, needle insertion bending experiments were conducted. Figure 14 shows the lab experiment setup. In the experiments, the developed L&T vibration device was used to insert a thin needle (made from a soft solder wire) of 1.0 mm diameter inserted into phantom tissues. The thin and soft solder wire is easily bent permanently, and good for experimental bending observation. The thin solder wire was inserted into a tissue phantom to 30 mm in depth at 6 mm/s, as shown in the left diagrams of Figure 14(a). All three scenarios were tested in the experiments. The ultrasonic driving power was set at 200 V. The results are shown in Figure 14(b). The proposed L&T vibration insertion was able to deliver the most accurate insertion that successfully reached the targeted insertion location with almost no deflection, as shown in the right diagram of Figure 14(b). The deflection is 2.331° for the needle with the traditional longitudinal vibration, and the deflection is 4.589° for the needle insertion without vibration assistance, as shown in Figure 14(b). The experiment observation confirms our hypothesis that without using vibration, larger tissue damage can be generated during the needle insertion. This is primarily due to the larger friction force end of causing larger tissue damages. Compare to the insertion with longitudinal vibration and the one without vibration assistance, the one with vibration assistance still performs better than the one without. In other words, the needle insertions with vibration assistance can achieve better results, and the one with the proposed combined L&T vibration assistance delivers the best result.

7 CONCLUSIONS

In this paper, a new wave-guided L&T vibration-assisted needle insertion device was presented for medical applications. To reduce the friction force during the insertion, L&T vibration is able to cyclic and instantaneous alter the amplitude and direction of the resultant insertion speed. Analytical modeling and design of the waveguide L&T transducer were discussed. Due to the complex geometric shape of the L&T transducer, SLM-AM was used to fabricate the transducer. Both the simulations and the laboratory experiments have demonstrated that the new waveguide-based L&T vibration-assisted insertion device can cause lower insertion force and more accurate insertion compared to longitudinal vibration actuated needles. The lab experiment results confirm that the presented waveguide-based L&T transducer is able to deliver much better vibration conversion and higher energy efficiency than the traditional methods. The presented device design and control method can be used for medical treatment applications, such as biopsy (for kidney, breast, and liver), brachytherapy (for prostate cancer treatments) or anesthetic procedures, to deliver high placement

accuracy and reduce patients' discomfort. The presented design and control method is also currently being used to explore the feasibility of flexible electrode insertions for neurology surgery treaments, as some of our preliminary results recently presented in [22].

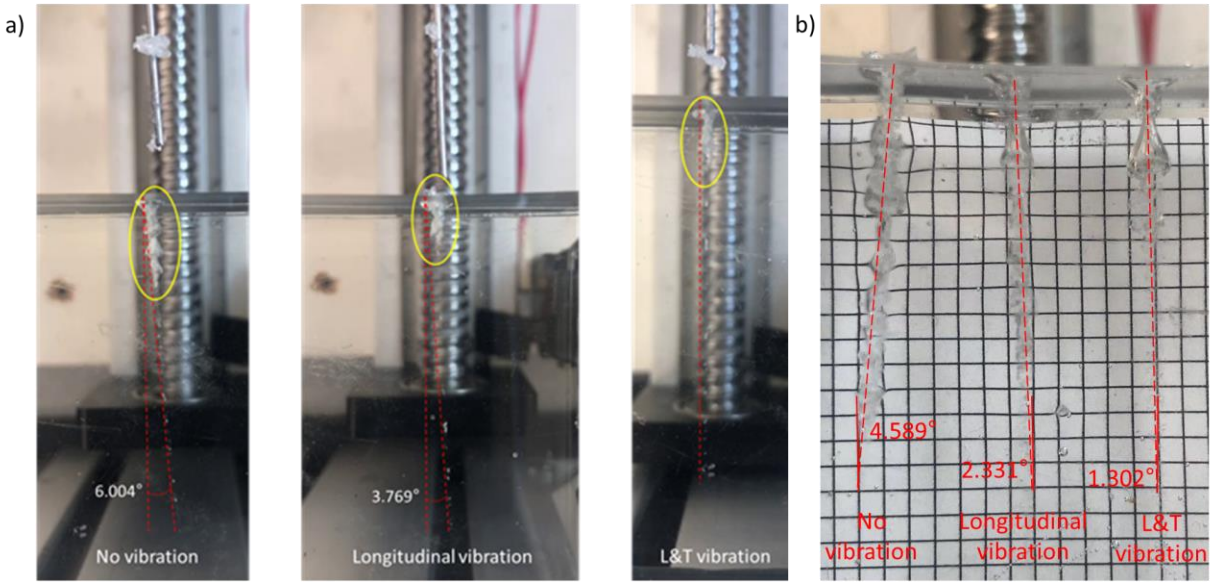

Figure 14: Insertion experiments with and without ultrasonic vibrations.

ACKNOWLEDGMENTS

The paper was partially supported by the National Science Foundation under Grant NSF-1938533 to NC State University as a sub-recipient. Their supports are greatly appreciated.

Yi Wang, http://orcid.org/0000-0002-7186-0855
Yi Cai, http://orcid.org/0000-0002-7587-8956
Yuan-Shin Lee, http://orcid.org/0000-0001-9892-5199

REFERENCES

[1] Abolhassani, N.; Patel, R.; Moallem, M.: Needle insertion into soft tissue: A survey, Medical Engineering & Physics, 29(4), 2007, 413–431. https://doi.org/10.1016/j.medengphy.2006.07.003.
[2] Al-Budairi, H.; Lucas, M.; Harkness, P.: A design approach for longitudinal–torsional ultrasonic transducers, Sensors and Actuators A: Physical, 198, 2013, 99–106. https://doi.org/10.1016/j.sna.2013.04.024.
[3] ANSYS (19.1). (2018). [Software]. https://www.ansys.com/
[4] Barnett, A. C.; Wolkowicz, K.; Moore, J. Z.: Vibrating Needle Cutting Force, V002T02A025, Volume 2: Processing, Detroit, Michigan, USA, 2014. https://doi.org/10.1115/MSEC2014-4049.
[5] Brandl, E.; Heckenberger, U.; Holzinger, V.; Buchbinder, D.: Additive manufactured AlSi10Mg samples using Selective Laser Melting (SLM): Microstructure, high cycle fatigue, and fracture behavior, Materials & Design, 34, 2012, 159–169. https://doi.org/10.1016/j.matdes.2011.07.067.

[6] Cai, Y.; Moore, J.; Lee, Y.-S.: Novel surgical needle design and manufacturing for vibratory-assisted insertion in medical applications, Computer-Aided Design and Applications, 14(6), 2017, 833–843. https://doi.org/10.1080/16864360.2017.1287759.
[7] Cai, Y.; Moore, J.; Lee, Y.-S.: Vibration Study of Novel Compliant Needle used for Vibration-assisted Needle Insertion, CAD&A, 16(4), 2018, 742–754. https://doi.org/10.14733/cadaps.2019.742-754.
[8] Casanova, F.; Carney, P. R.; Sarntinoranont, M.: In vivo evaluation of needle force and friction stress during insertion at varying insertion speed into the brain, Journal of Neuroscience Methods, 237, 2014, 79–89. https://doi.org/10.1016/j.jneumeth.2014.08.012.
[9] Cleary, R.; Lucas, M.: Comparison of Longitudinal-Mode and Longitudinal-Torsional Mode Ultrasonic Bone Biopsy Devices, 2018 IEEE International Ultrasonics Symposium (IUS), 2018, 1–9. https://doi.org/10.1109/ULTSYM.2018.8579919.
[10] Gutowski, P.; Leus, M.: The effect of longitudinal tangential vibrations on friction and driving forces in sliding motion, Tribology International, 55, 2012, 108–118. https://doi.org/10.1016/j.triboint.2012.05.023.
[11] Huang, Y. C.; Tsai, M. C.; Lin, C. H.: A piezoelectric vibration-based syringe for reducing insertion force, IOP Conference Series: Materials Science and Engineering, 42, 2012, 012020. https://doi.org/10.1088/1757-899X/42/1/012020.
[12] Liao, X.; Sadiq, M.; Corner, G.; Cochran, S.; Huang, Z.: Reduced penetration force through ultrasound activation of a standard needle: An experimental and computational study, 2013 IEEE International Ultrasonics Symposium (IUS), 2013, 1436–1439.
[13] Littmann, W.; Storck, H.; Wallaschek, J.: Sliding friction in the presence of ultrasonic oscillations: superposition of longitudinal oscillations, Archive of Applied Mechanics (Ingenieur Archiv), 71(8), 2001, 549–554. https://doi.org/10.1007/s004190100160.z
[14] Ni, H.; Wang, Y.; Gong, H.; Pan, L.; Li, Z. J.; D. Wang.: A novel free-form transducer for the ultra-precision diamond cutting of die steel, Int J Adv Manuf Technol, 95, 5–8, 2018, 2185–2192. https://doi.org/10.1007/s00170-017-1347-1.
[15] Simone, C.; Okamura, A. M.: Modeling of needle insertion forces for robot-assisted percutaneous therapy, Proceedings 2002 IEEE International Conference on Robotics and Automation (Cat. No.02CH37292), 2, 2002, 2085–2091. https://doi.org/10.1109/ROBOT.2002.1014848.
[16] Solidworks (Education Edition 2020–2021). (2019). [Software]. https://www.solidworks.com/
[17] Tan, L.; Jones, J. A.; Barnett, A. C.; Zhang, H.; Moore, J. Z.; Zhang, Q.: Force Model for Ultrasonic Needle Insertion, Experimental Techniques, 42(5), 2018, 499–508. https://doi.org/10.1007/s40799-018-0255-0.
[18] Tsai, C. C.; Tseng, C. H.: The effect of friction reduction in the presence of in-plane vibrations, Arch Appl Mech, 75, 2–3, 164–176, 2006. https://doi.org/10.1007/s00419-005-0427-0.
[19] Wang, Y.; Han, C.; Mei, D.; Xu, C.: Localized Microstructures Fabrication Through Standing Surface Acoustic Wave and User-Defined Waveguides, Volume 1: Additive Manufacturing; Manufacturing Equipment and Systems; Bio and Sustainable Manufacturing, Erie, Pennsylvania, USA, 2019, V001T05A005. https://doi.org/10.1115/MSEC2019-2879.
[20] Wang, Y.; Lee, Y.-S.; Cai, Y.; Sun, Y.; Gong, H.: Design of Ultrasonic Longitudinal-Torsional Vibrator Based on Waveguide Principle for Manufacturing and Medical Applications, Procedia Manufacturing, 48, 2020, 114–122. https://doi.org/10.1016/j.promfg.2020.05.027.
[21] Wang, Y.; Cai, Y.; Gong, H.; Lee, Y.-S.: Design and 3D Printing of Waveguide-based Ultrasonic Longitudinal-Torsional Transducers for Medical Needle Insertion, (under review), Submitted to Sensors and Actuators A: Physical, 2021.
[22] Wang, Y.; Shih, Y.Y.I.; Lee, Y.-S.: Vibration-Assisted Insertion of Flexible Cortical Neural Micro-Electrodes with Bio-Dissolvable Guides for Medical Implantation, (accepted for publication), The 2021 ASME 16th. International Manufacturing Science and Engineering Conference, MSEC2021, Virtual-Online, June 21-25, 2021, Paper No.: MSEC2021-63952, (11 pp).